Evidence for Intramolecular Permutation (Pseudorotation) at the Central Antimony Atom and Strong Equatophilicity of an Iron and a Ruthenium Ligand in Pentacoordinate Hypervalent Antimony Compounds

Koichiro Toyota, Yukiya Wakisaka, Yohsuke Yamamoto, and Kin-ya Akiba*

Department of Chemistry, Graduate School of Science, Hiroshima University, 1-3-1 Kagamiyama, Higashi-Hiroshima 739-8526, Japan

Received September 12, 2000

Diastereomeric pentacoordinate hypervalent stiboranes with an Sb−Fe bond {**4a** and **4b**: RfRfm*Sb*FeCp(CO)$_2$ {Rf = *o*-$C_6H_4C(CF_3)_2O$-, Rfm* = *o*-$C_6H_4C^*(CF_3)(Me)O$-} were synthesized by the reaction of stiboranide anion, RfRfm*Sb*$^-$Li$^+$ (**3-Li**), with CpFeI(CO)$_2$ in the presence of $AgBF_4$. The carbonyl group of **4** was replaced with triphenylphosphine by irradiation with a tungten lamp to give a mixture of four diastereomers {**5a**−**5d**: RfRfm*Sb*Fe*Cp(CO)(PPh$_3$)}. Each of the diastereomers was separated by TLC, and the relative stereochemistry was determined by X-ray crystallographic analysis. The thermal equilibration from the pure diastereomer of **5** indicated that the isomerization took place through inversion (pseudorotation) at the central antimony atom. The pseudorotational barriers of **5** were much higher than those of Rf$_2$Sb*Cl and RfRfm*Sb*(*p*-$CH_3C_6H_4$). These results are consistent with the electron-donating properties of the group 8 transition metal fragment. Hypervalent stiboranes {**6**, Rf$_2$Sb*Fe*Cp(CO)(PMe$_3$); **7**, Rf$_2$Sb*Fe*Cp(CO)(PEt$_3$)} were also prepared by similar procedures. The order of pseudorotational barriers [**2** {Rf$_2$Sb*Fe*Cp(CO)(PPh$_3$)} (32.8, 33.2 kcal/mol) > **7** (32.5, 32.9 kcal/mol) > **6** (32.2, 32.7 kcal/mol)] suggests that the steric effect of the iron ligand also played a role. The pseudorotational barriers of the corresponding ruthenium compounds, RfRfm*Sb*RuCp(CO)$_2$ (**12a** and **12b**), were slightly higher than those of the corresponding iron compounds (**4a** and **4b**).

Introduction

Synthesis and properties of compounds bearing a hypervalent group 15 element−transition metal bond have attracted interests recently.[1−11] However, many of the compounds obtained hitherto are unstable toward atmospheric moisture and systematic investigation of quantitative effects of the transition metal fragments on the properties of metalated hypervalent group 15 element compounds has not been carried out mainly because of the instabilty of these compounds. Among the properties of these compounds, the stereochemical rigidity of metalated pentacoordinate compounds is interesting for us because of the following observations: (i) The positional isomerization (pseudorotation) in pentacoordinate compounds is facile, especially in acyclic compounds.[12] (ii) The very low barrier of

(1) (a) Malisch, W.; Panster, P. *Angew. Chem., Int. Ed. Engl.* **1974**, *13*, 670. (b) Malisch, W.; Panster, P. *Chem. Ber.* **1975**, *108*, 700. (c) Malisch, W.; Kaul. H.-A.; Gross, E.; Thewalt, U. *Angew. Chem., Int. Ed. Engl.* **1982**, *21*, 549. *Angew. Chem. Supp.* **1982**, 1281.

(2) Matsumura, Y.; Harakawa, M.; Okawara, R. *J. Organomet. Chem.* **1974**, *71*, 403.

(3) (a) Wachter, J.; Mentzen, B. F.; Riess, J. G. *Angew. Chem., Int. Ed. Engl.* **1981**, *20*, 284. (b) Jeanneaux, F.; Grand, A.; Riess, J. G. *J. Am. Chem. Soc.* **1981**, *103*, 4272. (c) Dupart, J.-M.; Grand, A.; Pace, S.; Riess, J. G. *J. Am. Chem. Soc.* **1982**, *104*, 2316. (d) Dupart, J.-M.; Grand, A.; Riess, J. G. *J. Am. Chem. Soc.* **1986**, *108*, 1167.

(4) (a) Lattman, M.; Anand, B. N.; Garrett, D. R.; Whitener, M. A. *Inorg. Chim. Acta* **1983**, *76*, L139. (b) Lattman, M.; Morse, S. A.; Cowley, A. H.; Lasch, J. G.; Norman, N. C. *Inorg. Chem.* **1985**, *24*, 1364. (c) Lattman, M.; Chopra, S. K.; Cowley, A. H.; Arif, A. M. *Organometallics* **1986**, *5*, 677. (d) Burns, E. G.; Chu, S. S. C.; de Meester, P.; Lattman, M. *Organometallics* **1986**, *5*, 2383. (e) Lattman, M.; Burns, E. G.; Chopra, S. K.; Cowley, A. H.; Arif, A. M. *Inorg. Chem.* **1987**, *26*, 1926. (f) Khasnis, D. V.; Lattman, M.; Siriwardane, U. *J. Chen. Soc., Chem. Commun.* **1989**, 1538. (g) Khasnis, D. V.; Lattman, M.; Siriwardane, U. *Inorg. Chem.* **1989**, *28*, 681. (h) Khasnis, D. V.; Lattman, M.; Siriwardane, U. *Inorg. Chem.* **1989**, *28*, 2594. (i) Khasnis, D. V.; Lattman, M.; Siriwardane, U.; Chopra, S. K. *J. Am. Chem. Soc.* **1989**, *111*, 3103. (j) Khasnis, D. V.; Lattman, M.; Siriwardane, U. *Organometallics* **1991**, *10*, 1326. (k) Khasnis, D. V.; Lattman, M.; Siriwardane, U.; Zhang, H. *Organometallics* **1992**, *11*, 2074. (l) Khasnis, D. V.; Burton, J. M.; Zhang, H.; Lattman, M. *Organometallics* **1992**, *11*, 3745.

(5) (a) Ebsworth, E. A. V.; McManus, N. T.; Pilkington, N. J.; Rankin, D. W. H. *J. C. S.; Chem. Commun.* **1983**, 484. (b) Ebsworth, E. A. V.; Holloway, J. H.; Pilkington, N. J.; Rankin, D. W. H. *Angew. Chem., Int. Ed. Engl.* **1984**, *23*, 630.

(6) (a) Dixon, D. A.; Arduengo, A. J., III. *J. Am. Chem. Soc.* **1987**, *109*, 338. (b) Arduengo, A. J., III.; Lattman, M.; Dias, H. V. R.; Calabrese, J. C.; Kline, M. *J. Am. Chem. Soc.* **1991**, *113*, 1799.

(7) Anand, B. N.; Bains, R.; Usha, K. *J. Chem. Soc., Dalton Trans.* **1990**, 2315.

(8) (a) Chopra, S. K.; Martin, J. C. *Heteroatom Chem.* **1991**, *2*, 71. (b) Martin, J. C.; Chopra, S. K.; Moon, C. D.; Forbus, T. R.; Jr. *Phosphorus, Sulfur, Silicon Relat. Chem.* **1993**, *76*, 347.

(9) (a) Nakazawa, H.; Kubo, K.; Miyoshi, K. *J. Am. Chem. Soc.* **1993**, *115*, 5863. (b) Kubo, K.; Nakazawa, H.; Mizuta, T.; Miyoshi, K. *Organometallics* **1998**, *17*, 3522. (c) Nakazawa, H.; Kawamura, K.; Kubo, K.; Miyoshi, K. *Organometallics* **1999**, *18*, 2961.

(10) (a) Montgomery, C, D. *Phosphorus, Sulfur, Silicon* **1993**, *84*, 23. (b) Faw, R.; Montgomery, C, D.; Rettig, S. J.; Shurmer, B. *Inorg. Chem.* **1998**, *37*, 4136.

(11) (a) Yamamoto, Y.; Okazaki, M.; Wakisaka, Y.; Akiba, K.-y. *Organometallics* **1995**, *14*, 3364. (b) Toyota, K.; Yamamoto, Y.; Akiba, K.-y. *J. Chem. Res., Synop.* **1999**, 386. (c) Toyota, K.; Yamamoto, Y.; Akiba, K.-y. *Chem. Lett.* **1999**, 783.

10.1021/om000790l CCC: $19.00
Publication on Web 11/02/2000

Scheme 1

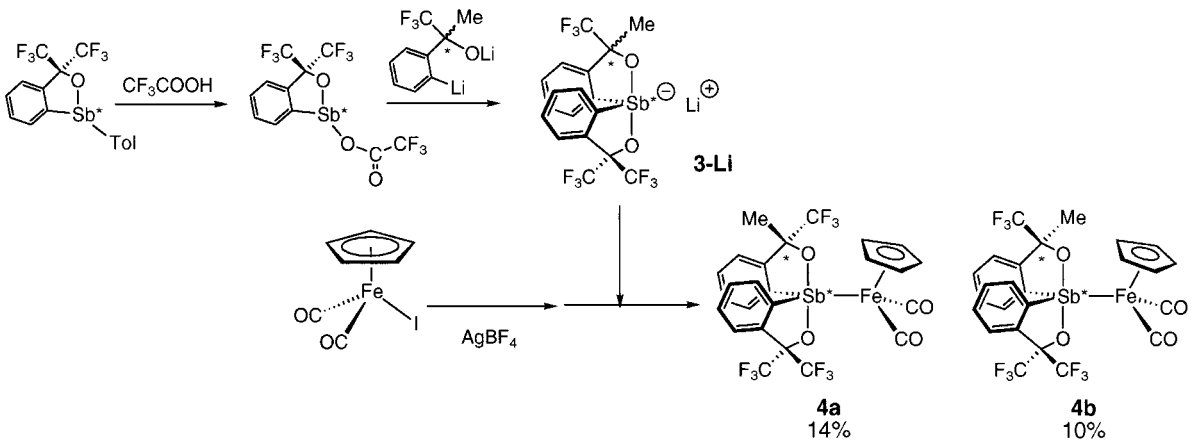

pseudorotation could be heightened by introduciton of bidentate ligands such as Martin ligand {Rf = *o*-$C_6H_4C(CF_3)_2O$-}. For example, chirality of spirocyclic phosphorane Rf_2P^*H with two Martin ligands remains stable even at room temperature.[13] (iii) However, even in the Rf_2M^*X compounds (M = group 15 element) the pseudorotational barrier is strongly dependent on the monodentate ligand (X), for example, the configuration of the central antimony in Rf_2Sb^*X with an electronegative atom (X = halogen) is not stable.[14,15] Recently we reported the synthesis and isomerization of stable diastereomeric hypervalent antimony compounds $Rf_2Sb^*Fe^*(Cp)(CO)(PPh_3)$ (**2a** and **2b**);[11a] the barrier of the isomerization between the diastereomers could be estimated to be very high on the basis of the very slow isomerization even at 140 °C, but the exact barrier was not obtained due to the partial decomposition of the compounds at higher temperatures around 140 °C. Although we believe that the isomerization took place via pseudorotation at the central antimony atom and the very high barrier should be ascribed to the electron-donating property of the iron fragment,[11a] other mechanisms are also possible for the isomerization between the diastereomers: (i) the Sb−Fe bond cleavage and recombination after isomerization of one of the fragment; (ii) the dissociation of one of the ligands on the iron group.

In this paper we report the synthesis of RfRfm*Sb*-Fe*Cp(CO)(PPh_3) (**5a**−**5d**: Rfm* = *o*-$C_6H_4C^*(CF_3)$-(Me)O-} with three chiral centers on the carbon, antimony, and iron atoms. Each diastereomer of **5** was isolated pure and was structurally characterized by X-ray analysis. The thermal equilibration from the pure diastereomer of **5** clearly showed that the isomerization did not take place through cleavage and recombination of the Sb−Fe bond or through dissociation and recoordination of one of the substituents on the iron atom but did through inversion (pseudorotation) at the central antimony atom.

In addition, $Rf_2Sb^*Fe^*Cp(CO)(PR_3)$ {**6** (R = Me) and **7** (R = Et)}, $Rf_2Sb^*RuCp(CO)_2$ (**9**), and RfRfm*Sb*RuCp-$(CO)_2$ (**12a** and **12b**) were prepared and the pseudorotational barriers were determined in order to investigate the effects of the group 8 ligands.

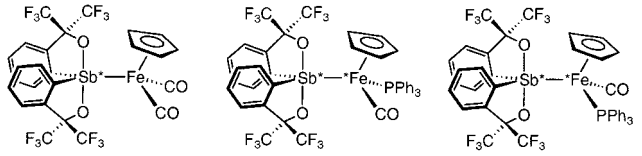

1 **2a** **2b**

Results and Discussion

Preparation of 4 {RfRfm*Sb*FeCp(CO)$_2$ (Rf = *o*-$C_6H_4C(CF_3)_2O$-, Rfm* = *o*-$C_6H_4C^*(CF_3)(Me)O$-)}. Reaction of a mixture of diastereomeric 10-Sb-4 stiboranide anion (**3-Li**)[16] with $CpFeI(CO)_2$[17] in the presence of $AgBF_4$ gave a diastereomeric mixture of RfRfm*Sb*Fe-$Cp(CO)_2$ (**4a** and **4b**) as outlined in Scheme 1.

These compounds were stable to atmospheric moisture and could be separated by TLC (SiO_2, CH_2Cl_2:*n*-hexane = 2:1). The relative stereochemistry of the compounds was determined by X-ray structural analysis (vide infra).

Preparation of Diastereomeric 5a−5d {RfRfm*Sb*Fe*Cp(CO)(PPh_3)}. Diastereomerically pure **4a** was irradiated under a tungsten lamp at room temperature in THF in the presence of 1.5 equiv of PPh_3 (Scheme 2). The reaction was monitored by ^{19}F NMR, showing that all of the diastereomers, **5a**−**5d**, were formed. A similar but slightly different ratio of **5a**−**5d** was obtained starting from diastereomerically pure **4b** as shown in Figure 1.

These compounds, **5a**−**5d**, were stable to atmospheric moisture and could be separated by TLC (SiO_2, CH_2Cl_2:hexane = 2.5:1). The relative stereochemistry of the compounds was determined by X-ray structural analysis (vide infra).

Formation of the diastereomeric mixture of **5** from diastereomerically pure **4** indicated that cleavage of the

(12) Holmes, R. R. *Pentacoordinate Phosphorus*, ACS Monograph Series 175 and 176; American Chemical Society: Washington, DC, 1980; Vols. 1 and 2. Hoffmann, R.; Howell, J. M.; Muetterties, E. L. *J. Am. Chem. Soc.* **1972**, *94*, 3407.

(13) (a) Kojima, S.; Kajiyama, K.; Akiba, K.-y. *Bull. Chem. Soc. Jpn.* **1995**, *68*, 1785. (b) Kojima, S.; Kajiyama, K.; Akiba, K.-y. *Tetrahedron Lett.* **1994**, *35*, 7037.

(14) Kojima, S.; Takagi, R.; Nakata, H.; Yamamoto, Y.; Akiba, K.-y. *Chem. Lett.* **1995**, 857.

(15) (a) Holmes, R. R. *J. Am. Chem. Soc.* **1978**, *100*, 433. (b) Buono, G.; Llinas, J. R. *J. Am. Chem. Soc.* **1981**, *103*, 4532. (c) Trippett, S. *Phosphorus Sulfur* **1976**, *1*, 89. (d) Trippett, S. *Pure Appl. Chem.* **1970**, 40.

(16) Akiba, K.-y.; Nakata, H.; Yamamoto, Y.; Kojima, S. *Chem. Lett.* **1992**, 1559.

(17) King, R. B.; Stone, F. G. *Inorg. Synth.* **1963**, *7*, 110.

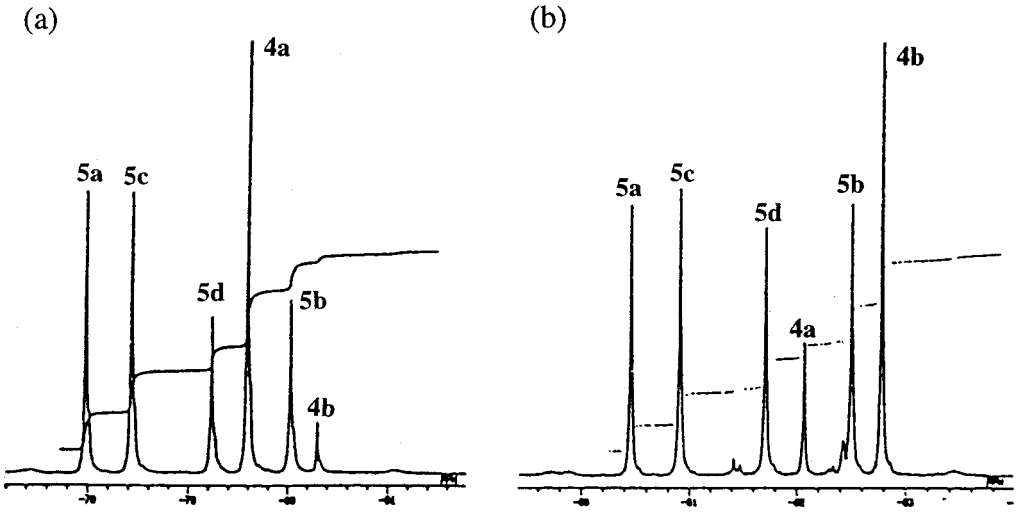

Figure 1. ^{19}F NMR spectrum of the reaction mixture in the photoreaction of **4** with 1.5 equiv of PPh_3 in THF: (a) **4a** was used as a starting material; (b) **4b** was used as a starting material.

Scheme 2

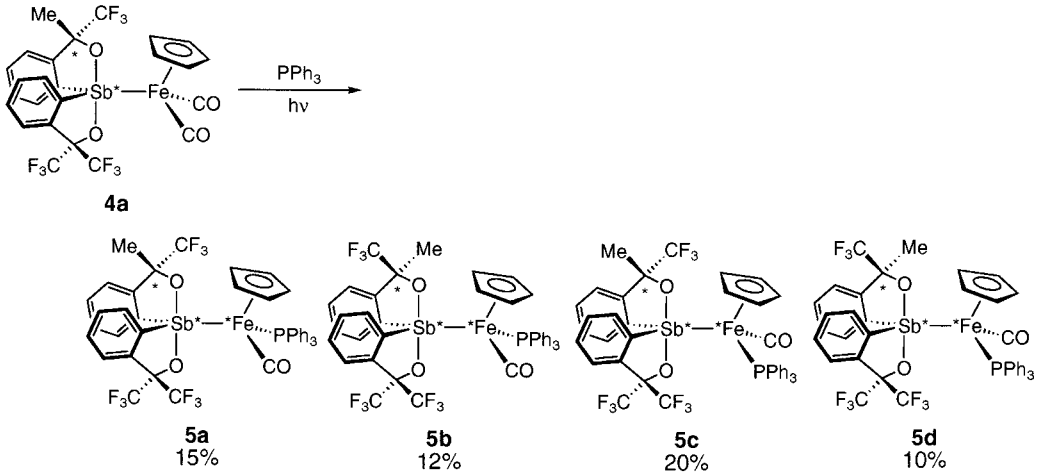

Sb−Fe bond took place during the photoreactions, because the thermal permutation of **4** (or **5**) was a very high energy process and the isomerization among diastereomers was observed only above 100 °C (vide infra). In the photoreaction, the Sb−Fe bond in **4** (or **5**) was cleaved at room temperature during the replacement of one of the two CO groups in **4** with triphenylphosphine to form a hypervalent antimony radical (**B**), which should be sterically labile on the basis of recent calculation[18] and should be easily isomerized to **B′** at the central antimony atom. Then the radical, **B** (or **B′**), recombined with the (caged) iron fragment [**C** (or **C′**)] to form a mixture of diastereomers of **4** (or **5**). In fact, a small amount of **4b** was observed in the reaction from **4a**, and **4a** was observed in the reaction from **4b** (Figure 1). Comparison of the spectrum of the reaction from **4a** with that from **4b** showed that the ratio of formation of **5a** and **5c** was larger than that of **5b** and **5d** in the reaction from **4a**. Since the relative stereochemistry of the antimony atom in **5a** and **5c** was the same as that in **4a**, the rate of the isomerization (**B** to **B′**) was not much faster than that of the recombination of caged radicals of **B** (or **B′**) and **C** (or **C′**) (Scheme 3).

X-ray Crystal Structures of 4a, 4b, 5a, 5b, and 5d. Crystals of **4a**, **4b**, **5a**, **5b**, and **5d** suitable for X-ray analysis were obtained by recrystallization from CH_2Cl_2−*n*-hexane for **4a**, benzene−*n*-hexane for **4b**, ether−methanol for **5a** and **5b**, and THF−*n*-hexane for **5d**, respectively. Figures 2−6 show the crystal structures of **4a**, **4b**, **5a**, **5b**, and **5d**. Selected bond lengths and bond angles for the structures of **4a**, **4b** (two independent molecules, which are similar in their structural parameters), **5a**, **5b**, and **5d** are listed in Table 1. The geometry about the antimony in **4a**, **4b**, **5a**, **5b**, and **5d** was roughly the same and could be considered as a distorted trigonal bipyramid (TBP) with the iron atom at the equatorial site of the TBP. Some disorder of the methyl group, that is, the disorder between structures of **D** and **E** (or **F** and **G**) (Figure 7), was observed in one of the two independent molecules of **4b** (30%) and **5a** (50%) (only major contributors are shown in Figures 2−6), but the relative stereochemistry of the three chiral centers was the same in the disordered structures and could be unambiguously established. Although the bond lengths of bonds a and b (in Table 1) were averaged by the disorder, bond a was always shorter than bond b in these compounds as shown in Table 1 (except **5a**, of which ratio of the disorder was 1:1). Similar results were observed in RfRfm*Sb*(*p*-$CH_3C_6H_4$).[19]

(18) Cramer, C. J. *J. Am. Chem. Soc.* **1990**, *112*, 7965.

(19) Kojima, S.; Doi, Y.; Okuda, M.; Akiba, K.-y. *Organometallics* **1995**, *14*, 1928.

Scheme 3

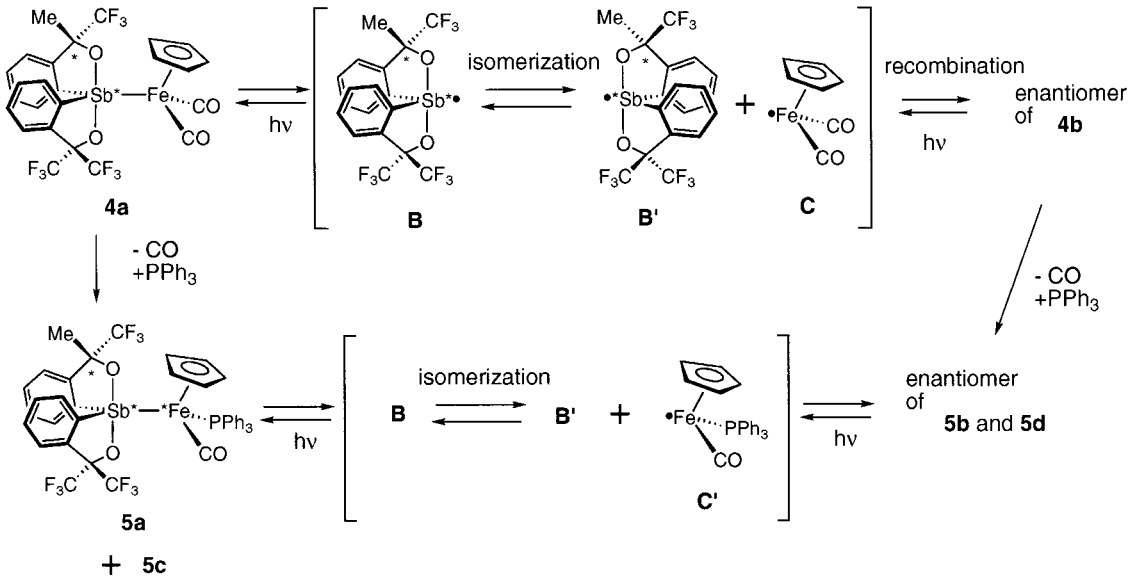

Table 1. Selected Bond Lengths and Bond Angles for 4a, 4b, 5a, 5b, 5d, 6a, 7a, 9, and 12a

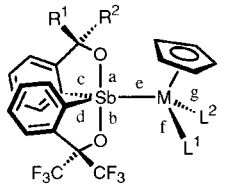

4a: M=Fe, R^1=Me, R^2=CF_3, L^1=L^2=CO
4b: M=Fe, R^1=CF_3, R^2=Me, L^1=L^2=CO
5a: M=Fe, R^1=Me, R^2=CF_3, L^1=CO, L^2=PPh_3
5b: M=Fe, R^1=CF_3, R^2=Me, L^1=CO, L^2=PPh_3
5d: M=Fe, R^1=CF_3, R^2=Me, L^1=PPh3, L^2=CO
6a: M=Fe, R^1=R^2=CF_3, L^1=CO, L^2=PMe_3
7a: M=Fe, R^1=R^2=CF_3, L^1=CO, L^2=PEt_3
9: M=Ru, R^1=R^2=CF_3, L^1=L^2=CO
12a: M=Ru, R^1=Me, R^2=CF_3, L^1=L^2=CO

	4a	4b		5a	5b	5d	6a	7a	9		12a
					Bond Lengths (Å)						
a	2.042(6)	2.079(10)	2.03(1)	2.10(2)	2.076(4)	2.074(5)	2.085(6)	2.108(6)	2.080(3)	2.085(3)	2.059(5)
b	2.102(5)	2.089(10)	2.077(10)	2.14(2)	2.133(4)	2.125(5)	2.156(6)	2.113(6)	2.089(3)	2.076(3)	2.109(5)
c	2.099(7)	2.11(1)	2.09(1)	2.21(3)	2.118(5)	2.112(7)	2.162(8)	2.158(10)	2.102(4)	2.112(5)	2.122(8)
d	2.106(6)	2.09(1)	2.13(1)	2.14(3)	2.123(5)	2.123(7)	2.103(9)	2.131(10)	2.103(4)	2.107(5)	2.121(4)
e	2.483(1)	2.487(3)	2.486(2)	2.514(4)	2.5287(8)	2.522(1)	2.494(2)	2.514(2)	2.5735(4)	2.5711(6)	2.574(9)
f	1.78(1)	1.73(3)	1.79(2)	1.68(5)	1.759(9)	2.221(2)	1.73(1)	1.73(1)	1.899(5)	1.886(6)	1.849(10)
g	1.76(1)	1.75(3)	1.74(2)	2.248(9)	2.233(2)	1.771(8)	2.187(3)	2.202(4)	1.886(6)	1.909(7)	1.86(1)
					Bond Angles (deg)						
ab	161.2(2)	165.3(4)	163.4(4)	155.6(10)	156.3(1)	159.5(2)	152.4(3)	156.0(3)	162.1(1)	160.3(1)	161.1(2)
cd	114.5(3)	112.4(5)	115.8(5)	113(1)	116.0(2)	112.8(3)	115.1(3)	108.0(4)	116.7(2)	116.7(2)	114.9(3)
ac	80.7(3)	80.2(5)	79.8(5)	78(1)	79.4(2)	79.1(3)	78.5(3)	77.3(3)	79.5(1)	79.8(1)	80.5(3)
bd	78.7(2)	78.9(5)	78.6(6)	80(1)	77.5(2)	78.6(3)	76.3(3)	77.9(3)	79.6(2)	79.6(2)	78.9(3)
ad	91.0(2)	92.1(5)	92.5(6)	87(1)	91.3(2)	89.5(3)	88.7(3)	88.6(3)	91.8(2)	89.0(3)	90.1(3)
bc	89.3(2)	92.4(5)	91.5(5)	87(1)	86.9(2)	90.1(2)	87.0(2)	88.9(2)	90.3(1)	91.0(2)	90.3(3)
ce	126.5(2)	124.3(6)	119.6(3)	119.5(8)	130.9(1)	131.5(2)	126.8(2)	130.4(3)	120.5(1)	119.1(1)	127.2(2)
de	119.0(2)	123.2(4)	124.6(4)	127.3(8)	112.4(1)	115.6(2)	118.1(2)	120.6(3)	122.7(1)	124.1(1)	118.0(2)
a**e**	98.4(2)	99.8(3)	96.5(3)	105.6(6)	107.36(9)	98.0(1)	102.1(2)	100.1(2)	95.99(9)	97.20(9)	97.8(2)
be	100.3(1)	94.9(3)	100.1(3)	98.5(6)	96.2(1)	102.2(1)	105.4(2)	103.8(2)	101.89(9)	102.5(1)	100.9(1)

Intramolecular Permutation (Pseudorotation) at the Central Antimony Atom in 5. With pure diastereomer **5** in hand, the thermal permutation process was monitored by ^{19}F NMR using diastereomerically pure samples. For example, **5d** in *o*-dichlorobenzene was heated to 140 °C and gave after an 8.5 h equilibration 0.39:1 of **5a** and **5d** in addition to trace amount of **5b**, **5c**, and decomposition product RfRfm*Sb*OH. Similarly, **5c** in *o*-dichlorobenzene was heated to 140 °C and gave after an 8.5 h equilibration 1.16:1 of **5b** and **5c** in addition to a trace of **5a**, **5d**, and decomposition product RfRfm*Sb*OH as shown in Figure 8. The same equilibrium ratios {0.39:1 (**5a**: **5d**) or 1.16:1 (**5b**: **5c**)} were observed when pure **5a** (or **5b**) was used instead of **5d** (or **5c**). These results clearly showed that the isomerization took place through inversion (pseudorotation) at the central antimony atom and the intramolecular permutation (pseudorotation) should be the exclusive pathway (Scheme 4). The decomposition was considered to take place via Sb−Fe bond cleavage, and the formation of very small amounts of **5b** and **5c** from **5d**, and **5a** and **5d** from **5c** would be due to recombination of the diradicals formed by cleavage of the Sb−Fe bond. But the cleavage of the Sb−Fe bond was only a very minor process in the thermal reactions. The pseudorotation barriers between **5a** and **5d**, **5b** and **5c**, and **4a** and **4b** were calculated to be 33.5 (from **5d** to **5a**), 32.7 (from **5a** to **5d**), 31.9 (from **5c** to **5b**), 32.0 (from **5b** to **5c**), 30.6 (from **4a** to **4b**), and 30.4 kcal/mol (from **4b** to **4a**) at 140 °C (413 K). The pseudorotational barriers were much higher than that of Rf_2Sb^*Cl (14.1 kcal/mol at 313 K in toluene)[14] and those of

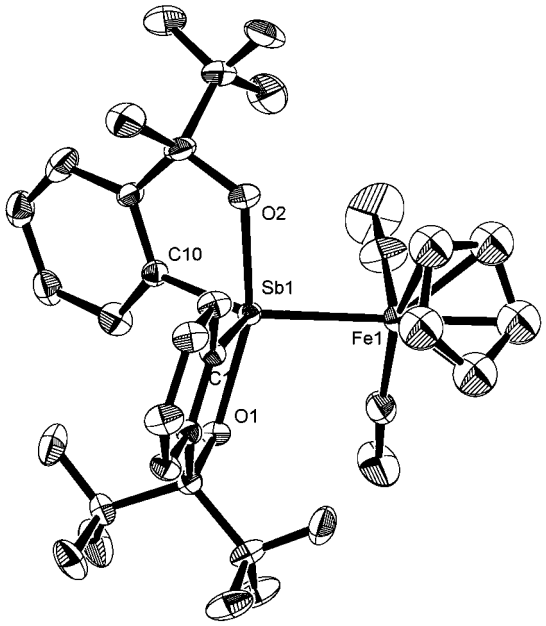

Figure 2. ORTEP diagram (30% probability ellipsoids) for **4a**.

Scheme 4

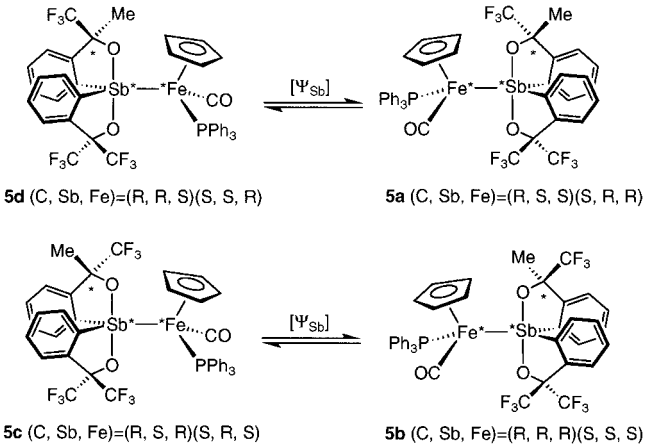

RfRfm*Sb*(*p*-$CH_3C_6H_4$) {28.3 kcal/mol (major to minor), 28.0 kcal/mol (minor to major) at 413 K in *o*-dichlorobenzene}.[19] The investigation is the first report to determine the effect of these iron fragments quantitatively, and the results could be explained by weak apicophilicity (strong equatophilicity) of the iron ligand because the energy barrier of intramolecular permutation (pseudorotation) has been considered to be determined by the apicophilicity (or equatophilicity) of the monodentate ligand in spirocyclic pentacoordinate compounds, and the energy of the transition state (or intermediate) **A** of the permutational process should be

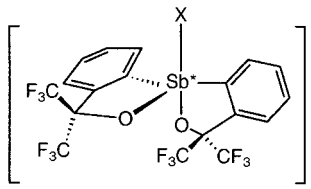

A

directly related with the apicophilicity of the monodentate ligand X.[12,14,15,19] Therefore, the apicophilicity

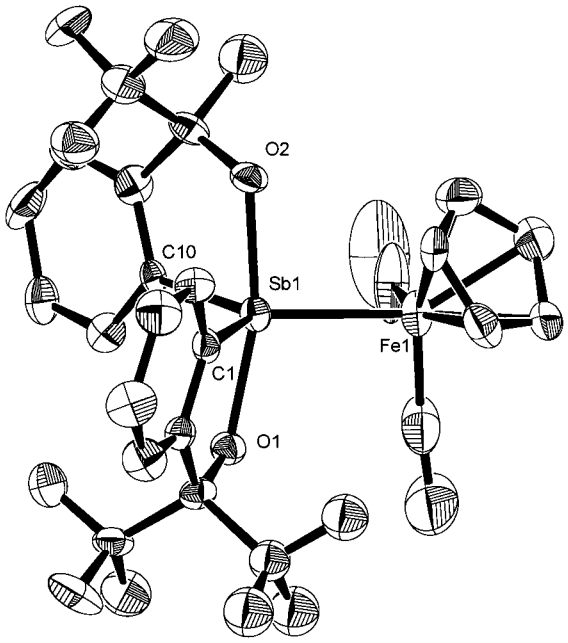

Figure 3. ORTEP diagram (30% probability ellipsoids) for **4b** (one of the independent molecules).

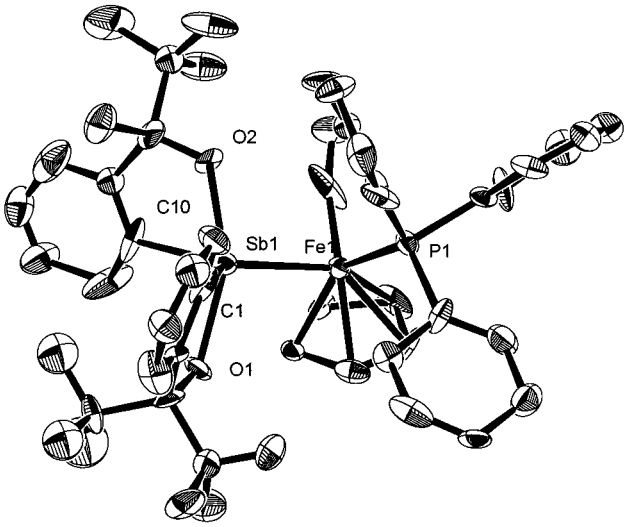

Figure 4. ORTEP diagram (30% probability ellipsoids) for **5a**.

of the group 8 transition metal fragments was confirmed to be smaller than that of the *p*-tolyl group by 2−5 kcal/mol estimated by the pseudorotational barriers of RfRfm*Sb*(*p*-$CH_3C_6H_4$), **4**, and **5**. These results are consistent with the electron-donating properties of the group 8 transition metal fragment. Although the result that the replacement of one of the two carbonyl groups with triphenylphosphine heightened the barrier was also consistent with the electronic effect (the stronger electron-donating effect of the phosphine than the carbonyl group), the pseudorotational barriers of trimethylphosphine- and triethylphosphine-substituted compounds, Rf_2Sb*Fe*Cp(CO)(PR_3) {**6** (R = Me) and **7** (R = Et)}, were investigated in order to see the steric and electronic effects of the substituent of the phosphine ligand.

Preparation and Pseudorotation of Rf_2Sb*Fe*Cp(CO)(PR_3) {6 (R = Me) and 7 (R = Et)}. Rf_2Sb*Fe*Cp-

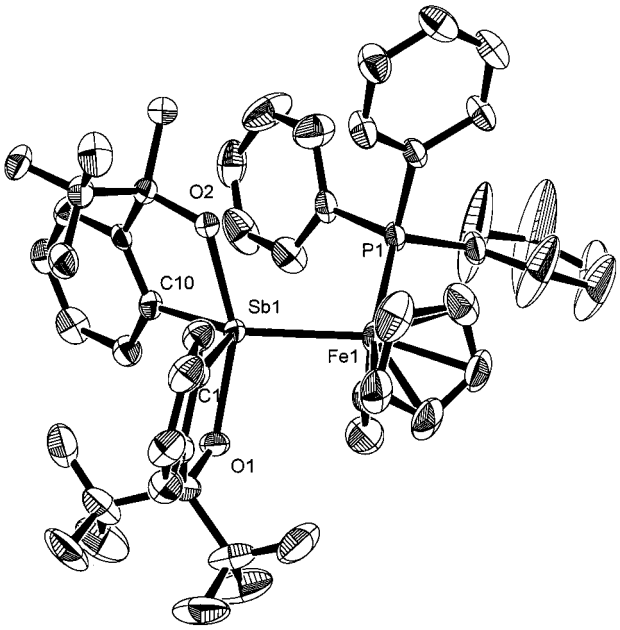

Figure 5. ORTEP diagram (30% probability ellipsoids) for **5b**.

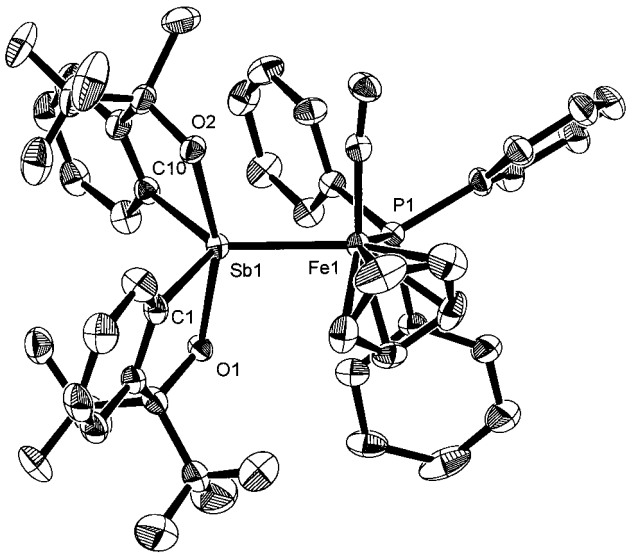

Figure 6. ORTEP diagram (30% probability ellipsoids) for **5d**.

(CO)(PR_3) {**6** (R = Me) and **7** (R = Et)} were prepared from **1** with irradiation of a tungsten lamp at room temperatue in 1,2-dichloroethane in the presence of PR_3 (Scheme 5).

These compounds are also stable to atmospheric moisture, and each of the diastereomers could be obtained pure after column chromatography (SiO_2, benzene:*n*-hexane = 1:1). The relative stereochemistry of **6** and **7** was determined by X-ray structural analysis of **6a** and **7a**. The ORTEP drawings of **6a** and **7a** are depicted in Figures 9 and 10.

The pseudorotational barriers of **6** and **7** were measured to be 32.2 (from **6a** to **6b**), 32.7 (from **6b** to **6a**), 32.5 (from **7a** to **7b**), and 32.9 kcal/mol (from **7b** to **7a**) in *o*-dichlorobenzene at 160 °C (433 K). The barriers of **2a** to **2b** and **2b** to **2a**[11a] were reexamined carefully by use of dried *o*-dichlorobenzene and were found to be 32.8 (from **2a** to **2b**) and 33.2 kcal/mol (from **2b** to **2a**) at 160 °C, that is, the order of the barriers was as follows: **2** (Ph_3P: 32.8, 33.2 kcal/mol) > **7** (Et_3P: 32.5, 32.9 kcal/mol) > **6** (Me_3P: 32.2, 32.7 kcal/mol). The results showed that the barriers were similar and very high, but the small difference was not consistent with the electronic effects of the ligand because electron-donating substituents should have hightened the barriers of pseudorotation, that is, the order of the barriers should be **7** > **6** > **2**.[12] Therefore, at least among the series of compounds with substituted phosphine, the experimental results indicated that steric effects of the substituents at the phosphorus played a role on the barriers; thus, the sterically bulkiest group, FeCp(CO)(PPh_3), had the highest energy barrier. The conclusion is consistent with the previous discussion[12] that apical positions in TBP are sterically more hindered than equatorial positions.

Preparation of $Rf_2Sb^*RuCp(CO)_2$ (9) and Rf-Rfm*Sb*RuCp(CO)$_2$ (12a and 12b) and Its Pseudorotation. $Rf_2Sb^*RuCp(CO)_2$ (**9**) and RfRfm*Sb*RuCp(CO)$_2$ (**12a** and **12b**) were prepared by procedures similar to those described above. $Rf_2Sb^{*-}Li^+$ (**8-Li**) was reacted with $CpRuI(CO)_2$[20] in the presence of $AgBF_4$ to afford **9** in 69% yield (Scheme 6). RfRfm*Sb*$^-$$Et_3HN^+$ (**11-Et$_3$HN**$^+$),[19] which was prepared from RfRfmH*Sb (**10**) and NEt_3, was reacted with $CpRuI(CO)_2$ in the presence of $AgBF_4$ to give **12a** and **12b** in 62% and 31%

Scheme 5

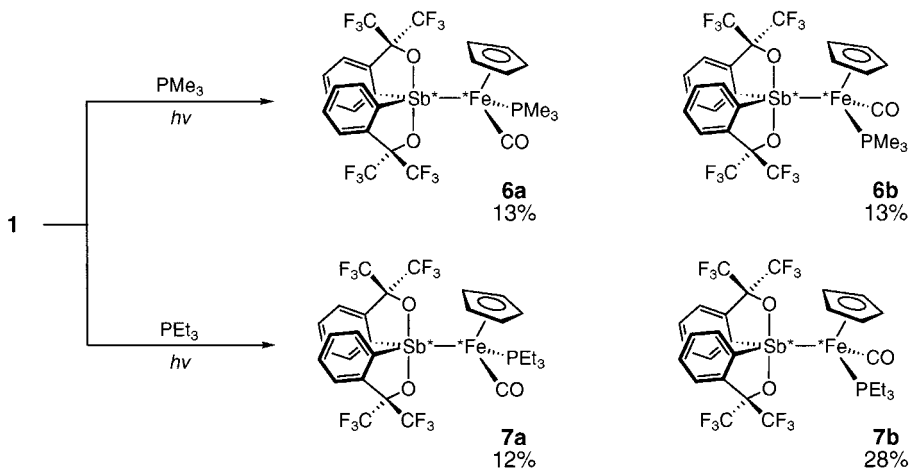

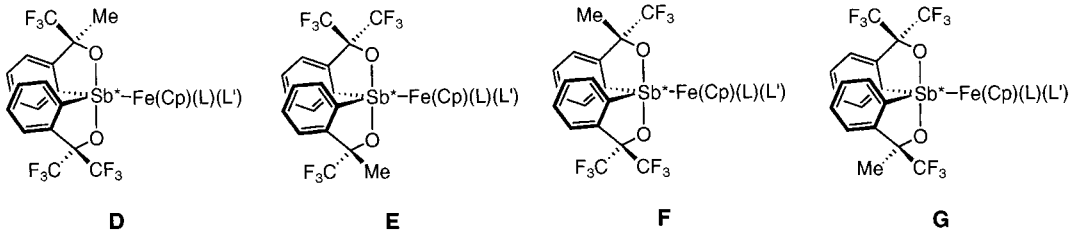

Figure 7. Disorder between structures of **D** and **E** (or **F** and **G**) in **4b** (**D**:**E** = 7:3) and **5a** (**F**:**G** = 1:1).

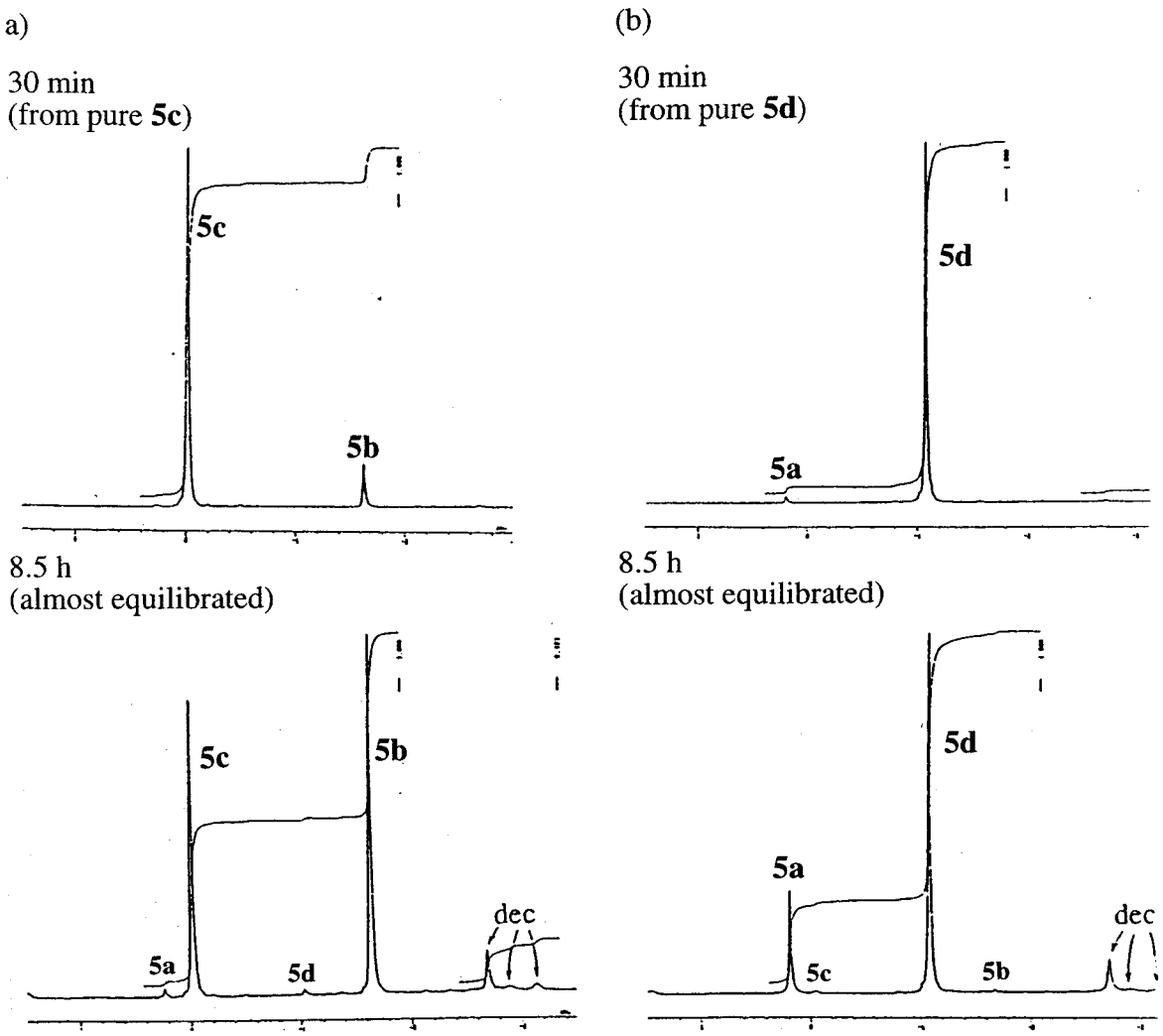

Figure 8. ^{19}F NMR spectrum of the reaction mixture in the thermal reactions of **5** in *o*-dichlorobenzene: (a) **5c** was used as a starting material; (b) **5b** was used as a starting material.

yields, respectively (Scheme 7). These compounds are stable to chromatographic treatment and were obtained pure after column chromatography (SiO_2, **9**; CH_2Cl_2, **12a** and **12b**; CH_2Cl_2:*n*-hexane = 1:1). X-ray crystallographic structures of **9** (two independent molecules, which are similar in their structural parameters) and **12a** revealed that the geometry around the antimony atom was very similar to those of the corresponding iron compounds. The ORTEP drawings of **9** and **12a** are depicted in Figures 11 and 12.

Rates of pseudorotation in **12a** to **12b** could be determined in *o*-dichlorobenzene at 110, 120, and 130 °C without significant decomposition. The activation parameters were calculated on the basis of the rates of pseudorotation at 110, 120, and 130 °C. The free energy of activation values at 110 °C ($\Delta G^{\ddagger}_{383}$) were 30.7 (from **12a** to **12b**) and 30.4 kcal/mol (from **12b** to **12a**), slightly higher than those of the corresponding iron compound (**4**) {$\Delta G^{\ddagger}_{383}$ = 30.5 (from **4a** to **4b**) and 30.2 kcal/mol (from **4b** to **4a**) at 110 °C}, and the activation entropy values ($\Delta S^{\ddagger}$) were slightly negative in both compounds [−6.2 (±0.4) (from **12a** to **12b**) and −6.5 (±0.1) (from **12b** to **12a**), −2.3 (±1.5) (from **4a** to **4b**) and −3.1 (±1.5) eu (from **4b** to **4a**)]. The small values of activation entropy suggested that the isomerization was a unimolecular process without cleavage of the Sb−Ru (or Sb−Fe) bond and was effected by pseudorotation at the central Sb atom also in **4** and **12**.

(20) Davison, A.; McCleverty, J. A.; Wilkinson, G. *J. Chem. Soc.* **1963**, 1133.

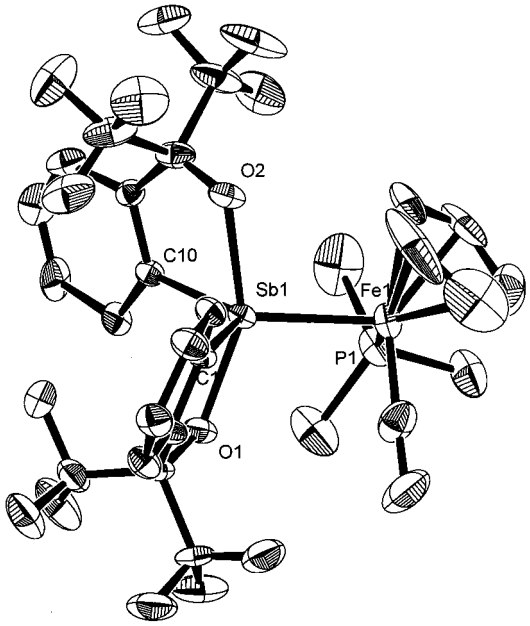

Figure 9. ORTEP diagram (30% probability ellipsoids) for **6a**.

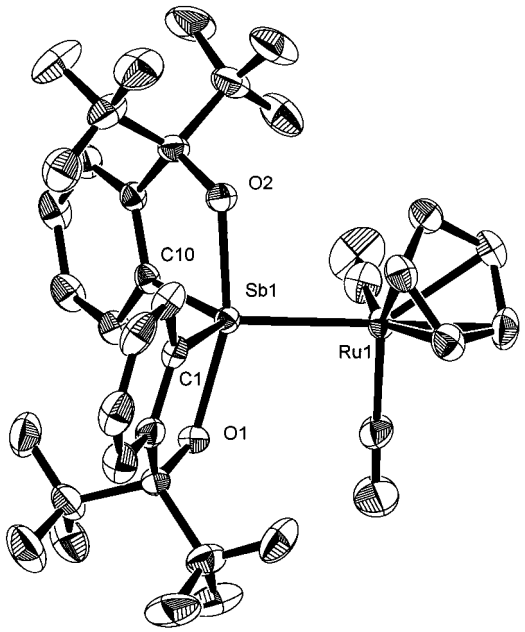

Figure 11. ORTEP diagram (30% probability ellipsoids) for **9** (one of the independent molecules).

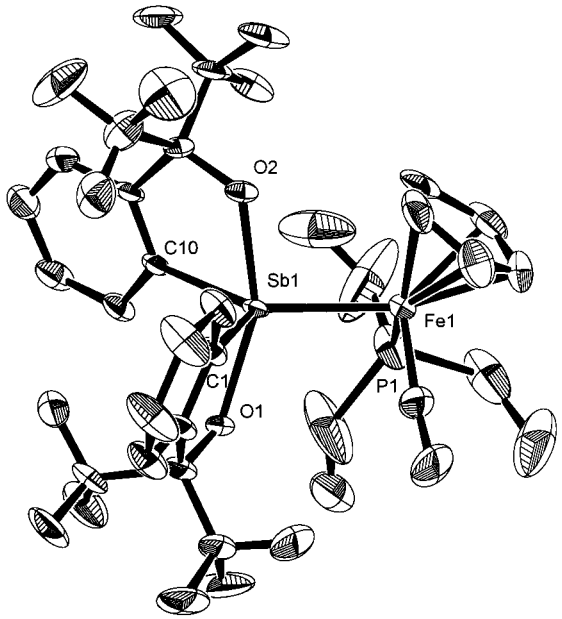

Figure 10. ORTEP diagram (30% probability ellipsoids) for **7a**.

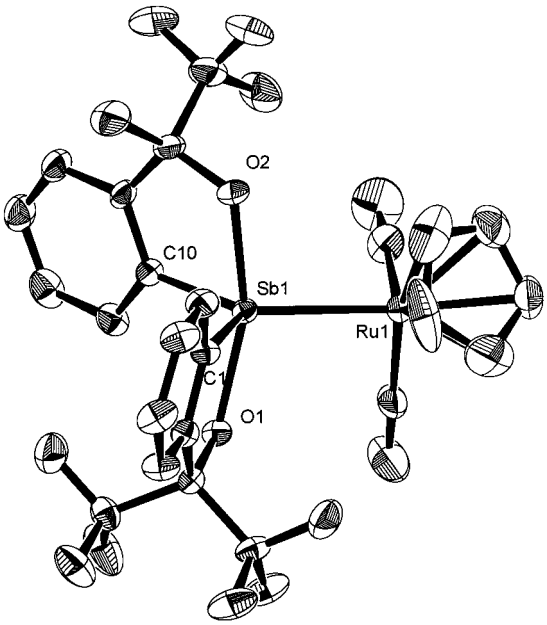

Figure 12. ORTEP diagram (30% probability ellipsoids) for **12a**.

To gain insight on the effect of different transition metal fragments on the pseudorotational barrier, hypervalent antimony compounds bearing a group 6 fragment were prepared and the pseudorotational barriers will be discussed in the following paper.[21]

In conclusion, we prepared various types of hypervalent antimony compounds bearing a group 8 (mainly iron) fragment, and the structures were unambiguously determined by X-ray analysis. The permutation among RfRfm*Sb*Fe*Cp(CO)(PPh_3) (**5a**−**5d**) was found to take place almost exclusively at the antimony atom, that is, the process should be intramolecular pseudorotation. The pseudorotational barriers of **5** were much higher than those of Rf_2Sb*Cl and RfRfm*Sb*(p-$CH_3C_6H_4$). These results are consistent with the electron-donating properties of the group 8 transition metal fragment. In addition, the steric effect of the substituents at the phosphorus also played a role in determining the pseudorotational barriers of RfRfm*Sb*Fe*Cp(CO)-(PR_3). The high barriers of pseudorotation of the corresponding ruthenium compounds, RfRfm*Sb*RuCp$(CO)_2$ (**12a** and **12b**), clearly showed that the transition metal group 8 fragments were strongly "equatophilic" and the stiboranes bearing the group 8 ligand were stereochemically rigid.

(21) Toyota, K.; Yamamoto, Y.; Akiba, K.-y. *Organometallics* **2000**, *19*, 5134.

Scheme 6

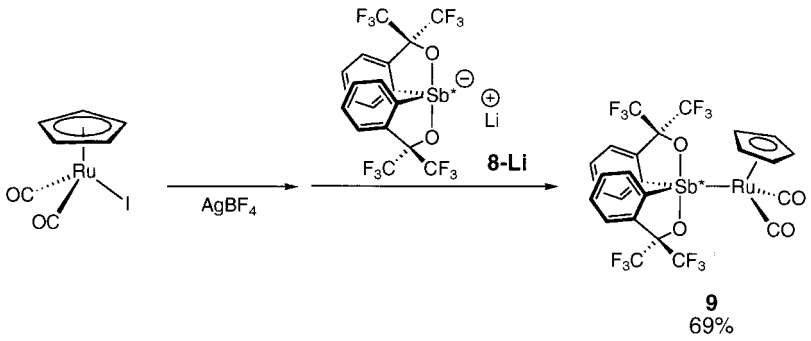

Scheme 7

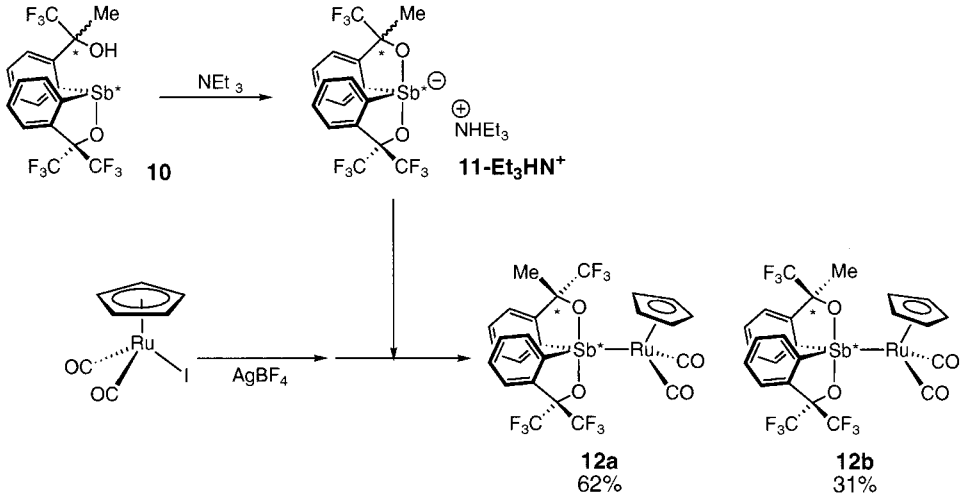

Experimental Section

Melting points were taken on a Yanagimoto micro melting point apparatus and are uncorrected. ^{1}H NMR (400-MHz), ^{19}F NMR (376-MHz), and ^{31}P NMR (162-MHz) spectra were recorded on a JEOL EX-400 spectrometer. Chemical shifts are reported (δ scale) from internal Me_4Si for ^{1}H, from external $CFCl_3$ for ^{19}F, or from external 85% H_3PO_4 for ^{31}P. IR spectra were recorded on a Shimadzu IR-460 or a FTIR-8100A spectrometer. Elemental analyses were performed on a Perkin-Elmer 2400CHN elemental analyzer. Flash column chromatography was carried out on Merck silica gel 7734 or 9385. Thin-layer chromatography was performed with Merck silica gel 7730 or GF-254 plates. All reactions were carried out under dry Ar.

Solvents and Reagents. THF were freshly distilled from sodium−benzophenone, and CH_2Cl_2, 1,2-dichloroethane, and *o*-dichlorobenzene were freshly distilled from CaH_2 under dry N_2. All other liquid reagents were also distilled from CaH_2 under dry N_2. The preparation of $CpFeI(CO)_2$[17] and $CpRuI(CO)_2$[20] followed published procedures. The preparations of RfSb*Tol[19] and lithium stiboranide 10-Sb-4 anion (**8-Li**$^+$)[16] have been reported.

RfRfm*Sb*FeCp(CO)$_2$ (4a, 4b). CF_3COOH (0.90 mL, 11.7 mmol) was slowly added to a solution of RfSb*Tol (3.00 g, 6.59 mmol) in 20 mL of dry CH_2Cl_2 at room temperature, and the mixture was stirred for 2 h. After the solvent and excess amounts of CF_3COOH were removed, the product, RfSb*(OC(O)CF_3), was dried in vacuo overnight. 1,1,1-Trifluoro-(2-bromophenyl)-2-propanol (1.22 mL, 6.59 mmol)[19] was treated with *n*-BuLi (8.24 mL, 13.2 mmol) in 16 mL of dry THF at −78 °C to room temperature overnight, and the mixture was added to the solution of RfSb*(OC(O)CF_3)[18] in 60 mL of dry THF at −78 °C. The mixture was stirred for 3.5 h and was added to the suspension generated from the reaction of $CpFeI(CO)_2$ (2.69 g, 8.85 mmol) and $AgBF_4$ (2.14 g, 11.0 mmol) in 20 mL of dry THF for 7 h. The mixture was heated under reflux for 13 h and was filtered through Celite. After the solvent was removed in vacuo, the crude products were subjected to TLC (SiO_2, CH_2Cl_2:*n*-hexane = 2:1) to separate the diastereomers **4a** (R_f = 0.67) and **4b** (R_f = 0.69). Suitable crystals of **4a** and **4b** for X-ray structural analysis were obtained by recrystallization from CH_2Cl_2−*n*-hexane and benzene−*n*-hexane, respectively. **4a**: 680 mg, 14%, orange plates, mp 206−207 °C (dec); IR (KBr) 2000, 2045 cm^{-1}; ^{1}H NMR ($CDCl_3$) 1.60 (s, 3 H), 5.13 (s, 5 H), 7.4−8.2 (m, 8 H); ^{19}F NMR ($CDCl_3$) −75.3 (q, 3 F, J = 9 Hz), −75.4 (q, 3 F, J = 9 Hz), −79.5 (s, 3 F). Anal. Calcd for $C_{25}H_{16}F_9O_4FeSb$: C, 41.19; H, 2.21. Found: C, 41.58; H, 1.98. **4b**: 465 mg, 10%, orange plates, mp 183−184 °C (dec); IR (KBr) 1993, 2000, 2040 cm^{-1}; ^{1}H NMR ($CDCl_3$) 1.67 (s, 3 H), 5.07 (s, 5 H), 7.4−8.2 (m, 8 H); ^{19}F NMR ($CDCl_3$) −75.2 (q, 3 F, J = 9 Hz), −76.1 (q, 3 F, J = 9 Hz), −80.1 (s, 3 F). Anal. Calcd for $C_{25}H_{16}F_9O_4FeSb$: C, 41.19; H, 2.21. Found: C, 41.41; H, 2.02.

RfRfm*Sb*Fe*Cp(PPh$_3$)(CO) (5a, 5b, 5c, and 5d). A solution of **4a** (438 mg, 0.60 mmol) and triphenylphosphine (244 mg, 0.93 mmol) in 7.5 mL of dry THF was irradiated with a tungsten lamp for 2 h at room temperature. After the solvent was evaporated the crude products were subjected to TLC (SiO_2, CH_2Cl_2:*n*-hexane = 2.5:1) to separate the diastereomers **5a** (R_f = 0.94), **5b** (R_f = 0.88), **5c** (R_f = 0.50), and **5d** (R_f = 0.44). **5a**: 86 mg, 15%, orange plates (recrystallized from ether−methanol), mp 230−231 °C (dec); IR (KBr) 1969 cm^{-1}; ^{1}H NMR ($CDCl_3$) 1.25 (s, 3 H), 4.79 (s, 5 H), 7.0−7.8 (m, 23 H); ^{19}F NMR ($CDCl_3$) −74.0 (q, 3 F, J = 9 Hz), −75.3 (q, 3 F, J = 9 Hz), −77.9 (s, 3 F); ^{31}P NMR ($CDCl_3$) δ 66.0 (s, 1 P). Anal. Calcd for $C_{42}H_{31}F_9O_3PFeSb$: C, 52.37; H, 3.24. Found: C, 52.34; H, 3.16. **5b**: 68 mg, 12%, orange plates (recrystallized from ether−methanol), mp 219−220 °C (dec); IR (KBr) 1965

cm^{-1}; ^{1}H NMR ($CDCl_3$) 1.47 (s, 3 H), 4.75 (s, 5 H), 7.1−7.8 (m, 23 H); ^{19}F NMR ($CDCl_3$) −74.1 (q, 3 F, J = 9 Hz), −75.8 (q, 3 F, J = 9 Hz), −80.0 (s, 3 F); ^{31}P NMR ($CDCl_3$) 67.0 (s, 1 P). Anal. Calcd for $C_{42}H_{31}F_9O_3PFeSb$: C, 52.37; H, 3.24. Found: C, 51.99; H, 3.02. **5c**: 118 mg, 20%, orange plates (recrystallized from ether), mp 232−235 °C (dec); IR (KBr) 1984 cm^{-1}; ^{1}H NMR ($CDCl_3$) 1.37 (s, 3 H), 4.48 (s, 5 H), 7.0−7.7 (m, 23 H); ^{19}F NMR ($CDCl_3$) −74.1 (q, 3 F, J = 9 Hz), −74.4 (q, 3 F, J = 9 Hz), −78.3 (s, 3 F); ^{31}P NMR ($CDCl_3$) 67.4 (s, 1 P). Anal. Calcd for $C_{42}H_{31}F_9O_3PFeSb$: C, 52.37; H, 3.24. Found: C, 52.51; H, 3.12. **5d**: 57 mg, 10%, orange plates (recrystallized from THF−*n*-hexane), mp 238−241 °C (dec); IR (KBr) 1961 cm^{-1}; ^{1}H NMR ($CDCl_3$) 1.63 (s, 3 H), 4.41 (s, 5 H), 6.9−8.0 (m, 23 H); ^{19}F NMR ($CDCl_3$) −73.8 (q, 3 F, J = 9 Hz), −75.0 (q, 3 F, J = 9 Hz), −79.1 (s, 3 F); ^{31}P NMR ($CDCl_3$) 67.7 (s, 1 P). Anal. Calcd for $C_{42}H_{31}F_9O_3PFeSb$: C, 52.37; H, 3.24. Found: C, 53.40; H, 3.74.

Rf_2Sb*Fe*Cp(PMe_3)(CO) (6a and 6b). A solution of **1** (536 mg, 0.68 mmol) and trimethylphosphine (0.07 mL, 0.68 mmol) in 40 mL of dry 1,2-dichloroethane was irradiated with a tungsten lamp for 6 h at room temperature. After the solvent was removed, the crude products were subjected to flash column chromatography (SiO_2, benzene:*n*-hexane = 1:1) to separate the diastereomers **6a** and **6b**. **6a**: 72 mg, 13%, orange plates (recrystallized from CH_2Cl_2−*n*-hexane), mp 268−272 °C (dec); IR (KBr) 1979 cm^{-1}; ^{1}H NMR ($CDCl_3$) 1.45 (d, 3 H, $^2J_{P-H}$ = 9.7 Hz), 4.79 (d, 5 H, $^3J_{P-H}$ = 1.9 Hz), 7.43 (t, 2 H, J = 7.3 Hz), 7.52 (t, 2 H, J = 7.3 Hz), 7.64 (d, 2 H, J = 7.3 Hz), 8.09 (d, 2 H, J = 7.3 Hz); ^{19}F NMR ($CDCl_3$) −74.2 (q, 6 F, J = 9 Hz), −75.4 (q, 6 F, J = 9 Hz); ^{31}P NMR ($CDCl_3$) 30.4 (s, 1 P). Anal. Calcd for $C_{27}H_{22}F_{12}O_3PFeSb$: C, 39.02; H, 2.67. Found: C, 39.00; H, 2.53. **6b**: 75 mg, 13%, orange plates (recrystallized from CH_2Cl_2−*n*-hexane), mp 275−279 °C (dec); IR (KBr) 1986 cm^{-1}; ^{1}H NMR ($CDCl_3$) 1.59 (d, 3 H, $^2J_{P-H}$ = 10.3 Hz), 4.65 (bs, 5 H), 7.44 (t, 2 H, J = 7.3 Hz), 7.53 (t, 2 H, J = 7.3 Hz), 7.65 (d, 2 H, J = 7.3 Hz), 8.09 (d, 2 H, J = 7.3 Hz); ^{19}F NMR ($CDCl_3$) −74.4 (q, 6 F, J = 9 Hz), −75.4 (q, 6 F, J = 9 Hz); ^{31}P NMR ($CDCl_3$) 31.0 (s, 1 P). Anal. Calcd for $C_{27}H_{22}F_{12}O_3PFeSb$: C, 39.02; H, 2.67. Found: C, 39.03; H, 2.43.

Rf_2Sb*Fe*Cp(PEt_3)(CO) (7a and 7b). By use of procedures similar to those of **6a** and **6b**, the diastereomers **7a** and **7b** were obtained from **1** (187 mg, 0.24 mmol) and triethylphosphine (1.0 M in THF, 0.24 mL, 0.24 mmol). **7a**: 25 mg, 12%, orange plates (recrystallized from CH_2Cl_2−*n*-hexane), mp 240−244 °C (dec); IR (KBr) 1971 cm^{-1}; ^{1}H NMR ($CDCl_3$) 1.00−1.10 (m, 9 H), 1.69−1.85 (m, 6 H), 4.85 (d, 5 H, $^3J_{P-H}$ = 1.5 Hz), 7.42 (t, 2 H, J = 7.3 Hz), 7.51 (t, 2 H, J = 7.3 Hz), 7.62 (d, 2 H, J = 7.3 Hz), 8.08 (d, 2 H, J = 7.3 Hz); ^{19}F NMR ($CDCl_3$) −74.2 (q, 6 F, J = 9 Hz), −75.4 (q, 6 F, J = 9 Hz); ^{31}P NMR ($CDCl_3$) 53.1 (s, 1 P). Anal. Calcd for $C_{30}H_{28}F_{12}O_3PFeSb$: C, 41.27; H, 3.23. Found: C, 41.20; H, 3.05. **7b**: 58 mg, 28%, orange plates (recrystallized from CH_2Cl_2−*n*-hexane); mp 245−250 °C (dec); IR (KBr) 1975 cm^{-1}; ^{1}H NMR ($CDCl_3$) 1.00−1.10 (m, 9 H), 1.77−1.84 (m, 3 H), 1.91−2.00 (m, 3 H), 4.67 (d, 5 H, $^3J_{P-H}$ = 1.5 Hz), 7.43 (t, 2 H, J = 7.8 Hz), 7.52 (t, 2 H, J = 7.8 Hz), 7.64 (d, 2 H, J = 7.8 Hz), 8.10 (d, 2 H, J = 7.8 Hz); ^{19}F NMR ($CDCl_3$) −74.1 (q, 6 F, J = 9 Hz), −75.2 (q, 6 F, J = 9 Hz); ^{31}P NMR ($CDCl_3$) 53.9 (s, 1 P). Anal. Calcd for $C_{30}H_{28}F_{12}O_3PFeSb$: C, 41.27; H, 3.23. Found: C, 41.27; H, 3.33.

Rf_2Sb*RuCp($CO)_2$ (9). A mixture of $CpRuI(CO)_2$ (349 mg, 1.0 mmol) and $AgBF_4$ (280 mg, 1.0 mmol) in 15 mL of THF was stirred for 2 h at room temperature. To the suspension was added **8-Li**$^+$ (613 mg, 1.0 mmol). The mixture was stirred for 20 h at room temperature and was filtered through Celite. After the solvent was removed in vacuo, the crude products were subjected to flash column chromatography (SiO_2, CH_2Cl_2) to give **9**. Suitable crystals of **9** for X-ray structural analysis were obtained by recrystallization from CH_2Cl_2−*n*-hexane. **9**: 575 mg, 0.69 mmol, 69%, colorless plate; mp 215−216 °C; IR (KBr) 2017, 2029, 2066 cm^{-1}; ^{1}H NMR ($CDCl_3$) 5.47 (s, 4 H), 7.52 (t, 2 H, J = 7.3 Hz), 7.60 (t, 2 H, J = 7.3 Hz), 7.72 (d, 2 H, J = 7.3 Hz), 8.16 (d, 2 H, J = 7.3 Hz); ^{19}F NMR ($CDCl_3$) −75.4 (q, 6 F, J = 9 Hz), −75.9 (q, 6 F, J = 9 Hz). Anal. Calcd for $C_{25}H_{13}F_{12}O_4SbRu$: C, 36.26; H, 1.58. Found: C, 36.16; H, 1.75.

RfRfm*Sb*RuCp($CO)_2$ (12a and 12b). A mixture of $CpRuI(CO)_2$[20] (153 mg, 0.44 mmol) and $AgBF_4$ (114 mg, 0.58 mmol) in 5 mL of THF was stirred for 3 h at room temperature. To the suspension was added **11-Et_3HN^+** generated from RfRfmHSb[19] (**10**; 200 mg, 0.36 mmol) and NEt_3 (51 mL, 0.37 mmol) in 5 mL of THF for 15 min at room temperature The mixture was stirred for 20 h at room temperature and was filtered through Celite. After the solvent was removed in vacuo, the crude products were subjected to flash column chromatography (SiO_2, CH_2Cl_2:*n*-hexane = 1:1) to separate the diastereomers **12a** and **12b**. Suitable crystals of **12a** for X-ray structural analysis were obtained by recrystallization from CH_2Cl_2−*n*-hexane. **12a**: 173 mg, 0.224 mmol, 62% (based on Sb), colorless plate; mp 211−212 °C; IR (KBr) 2005, 2059 cm^{-1}; ^{1}H NMR ($CDCl_3$) 1.60 (s, 3 H), 5.49 (s, 5 H), 7.4−7.7 (m, 6 H), 8.08 (d, 1 H, J = 7.8 Hz), 8.22 (d, 1 H, J = 7.8 Hz); ^{19}F NMR ($CDCl_3$) −75.3 to −75.1 (m, 6 F), −79.4 (s, 3 F). Anal. Calcd for $C_{25}H_{16}F_9O_4RuSb$: C, 38.78; H, 2.08. Found: C, 38.81; H, 2.06. **12b**: 575 mg, 0.69 mmol, 69% (based on Sb), colorless plate; mp 179−180 °C; IR (KBr) 2003, 2055 cm^{-1}; ^{1}H NMR ($CDCl_3$) 1.65 (s, 3 H), 5.44 (s, 5 H), 7.4−7.7 (m, 6 H), 8.11 (d, 1 H, J = 7.8 Hz), 8.15 (d, 1 H, J = 7.8 Hz); ^{19}F NMR ($CDCl_3$) −75.0 (q, 3 F, J = 9 Hz), −76.0 (q, 3 F, J = 9 Hz), −80.0 (s, 3 F). Anal. Calcd for $C_{25}H_{16}F_9O_4RuSb$: C, 38.78; H, 2.08. Found: C, 38.78; H, 1.87.

Measurements of Positional Isomerization via Berry Pseudorotation. (i) From 4a to 4b and from 4b to 4a. Solutions of **4a** and **4b** (ca. 10 mg, respectively) in 0.6 mL of dry *o*-dichlorobenzene were sealed in NMR tubes under dry N_2. The temperatures for the kinetic runs were maintained at 100 (± 1), 110 (± 1), 120 (± 1), and 130 (± 1) °C in an NMR probe. The composition of the diastereomers was monitored by integration of ^{19}F NMR signals. The data were analyzed assuming first-order kinetics. **(ii) From 5c to 5b and from 5d to 5a.** Solutions of **5c** (11.2 mg) and **5d** (11.4 mg) in 0.6 mL of *o*-dichlorobenzene were sealed in NMR tubes under dry N_2. The temperatures for the kinetic runs were maintained at 140 (± 1) °C in an NMR probe. The composition of the diastereomers was monitored by integration of ^{19}F NMR signals. The data were analyzed assuming first-order kinetics. **(iii) From 2a (6a, 7a) to 2b (6b, 7b).** Solutions of **2a**, **6a**, and **7a** (ca. 10 mg, respectively) in 0.6 mL of *o*-dichlorobenzene were sealed in NMR tubes under dry N_2. The temperatures for the kinetic runs were maintained at 160 (± 1) °C in an NMR probe. The composition of the diastereomers was monitored by integration of ^{19}F NMR signals. The data were analyzed assuming first-order kinetics. **(iv) From 12a to 12b.** Solutions of **12a** (ca. 10 mg) in 0.6 mL of *o*-dichlorobenzene were sealed in NMR tubes under dry N_2. The temperatures for the kinetic runs were maintained at 110 (± 1), 120 (± 1), and 130 (± 1) °C in an NMR probe. The composition of the diastereomers was monitored by integration of ^{19}F NMR signals. The data were analyzed assuming first-order kinetics.

Crystal Structures of 4a, 4b, 5a, 5b, 5d, 6a, 7a, 9, and 12a. Crystal data and numerical details of the structure determinations are given in Table 2. Crystals suitable for X-ray structure determination were mounted on a Mac Science MXC3 diffractometer and irradiated with graphite-monochromated Mo Kα radiation (λ = 0.71073 Å) (for **4a**, **4b**, **5a**, **5b**, **5d**, and **6a**) or Cu Kα radiation (λ = 1.54178 Å) (for **7a**) for data collection. Lattice parameters were determined by least-squares fitting of 31 reflections with 31° < 2θ < 35° in **4a**, of 20 reflections with 19° < 2θ < 25° in **4b**, of 31 reflections with 16° < 2θ < 28° in **5a**, of 31 reflections with 26° < 2θ < 36° in **5b**, of 31 reflections with 26° < 2θ < 30° in **5d**, of 31 reflections with 31° < 2θ < 35° in **6a**, of 31 refrections with 55° < 2θ < 60° in **7a**, of 31 refrections with 55° < 2θ < 60° in **12a**. Data

Table 2. Crystal Data for 4a, 4b, 5a, 5b, 5d, 6a, 7a, 9, and 12a

	4a	4b	5a	5b	5d	6a	7a	9	12a
formula	$C_{25}H_{16}O_4F_9FeSb$	$C_{25}H_{16}O_4F_9FeSb$	$C_{42}H_{31}O_3F_9FePSb$	$C_{42}H_{31}O_3F_9FePSb$	$C_{42}H_{31}O_3F_9FePSb$	$C_{27}H_{22}O_3F_{12}FePSb$	$C_{30}H_{28}O_3F_{12}FePSb$	$C_{25}H_{13}O_4F_{12}RuSb$	$C_{25}H_{16}O_4F_9RuSb$
mol wt	728.90	728.90	963.30	963.30	963.30	831.03	872.76	828.20	774.20
cryst syst	orthorhombic	monoclinic	monoclinic	triclinic	monoclinic	monoclinic	monoclinic	monoclinic	orthorhombic
space group	$P2_12_12_1$	$P2_1/n$	$P2_1/n$	$P\bar{1}$	$C2/c$	$P2_1/n$	$P2_1/n$	$P2_1/a$	$P2_12_12_1$
cryst dimens, mm	0.95 × 0.85 × 0.60	0.65 × 0.25 × 0.08	0.40 × 0.20 × 0.10	0.80 × 0.65 × 0.50	0.70 × 0.40 × 0.15	0.35 × 0.30 × 0.20	0.45 × 0.35 × 0.20	0.80 × 0.60 × 0.50	1.00 × 0.60 × 0.50
a, Å	14.814(3)	19.47(1)	21.094(6)	8.935(7)	20.612(8)	18.60(1)	19.861(6)	19.204(9)	14.943(6)
b, Å	20.675(4)	16.27(1)	12.557(3)	11.719(3)	25.75(1)	14.227(7)	14.810(5)	17.231(9)	20.774(9)
c, Å	8.521(2)	18.38(1)	15.120(4)	19.544(6)	17.430(7)	11.412(5)	11.110(4)	18.112(8)	8.545(5)
α, deg	90	90	90	73.68(2)	90	90	90	90	90
β, deg	90	115.78(4)	100.28(2)	84.55(4)	116.53(3)	91.56(4)	94.54(3)	114.77(3)	90
γ, deg	90	90	90	82.46(4)	90	90	90	90	90
V, Å^3	2609.9(1)	5241.5(1)	3941.0(1)	1943.3(1)	8276.7(1)	3018.3(1)	3257.7(1)	5441.9(1)	2652.7(1)
Z	4	8	4	2	8	4	4	8	4
D_{calc}, g cm^{-3}	1.855	1.847	1.623	1.646	1.546	1.84	1.780	2.021	1.938
abs coeff, cm^{-1}	1.6896	1.6825	1.1763	1.1926	1.1201	1.5337	11.733	1.6542	1.6745
F(000)	1424	2848	1920	960	3840	1632	1728	3184	1496
radiation, λ, Å	Mo Kα; 0.710 73	Mo Kα; 0.710 73	Mo Kα; 0.710 73	Mo Kα; 0.710 73	Mo Kα; 0.710 73	Mo Kα; 0.710 73	Cu Kα; 1.541 78	Mo Kα; 0.710 73	Mo Kα; 0.710 73
temp, K	298	298	298	298	298	298	298	298	298
2θ max, deg	60	55	55	55	55	55	130	55	55
scan rate, deg/min	3.0	2.0	1.5	5.0	6.0	4.0	5.0	6.0	2.0
linear decay, %	5.683	7.324	4.418	1.793	5.463		4.880	2.233	2.316
data collcd	$+h, +k, +l$	$+h, -k, \pm l$	$+h, +k, \pm l$	$-h, \pm k, \pm l$	$\pm h, +k, +l$	$+h, +k, \pm l$	$\pm h, +k, +l$	$+h, +k, \pm l$	$+h, +k, +l$
tot. data collcd, unique, obsd	4820, 4767, 4294 ($I > 3\sigma(I)$)	7277, 6957, 3975 ($I > 3\sigma(I)$)	5394, 5175, 2412 ($I > 3\sigma(I)$)	9594, 8922, 7456 ($I > 3\sigma(I)$)	9944, 9531, 6709 ($I > 3\sigma(I)$)	6107, 5973, 5441 ($I > 3\sigma(I)$)	5800, 5432, 4166 ($I > 3\sigma(I)$)	12993, 12484, 9833 ($I > 3\sigma(I)$)	3482, 3446, 2942 ($I > 3\sigma(I)$)
R int	0.019	0.025	0.025	0.015	0.021	0.088	0.058	0.011	0.009
no. of params refined	324	671	491	514	514	406	433	775	361
R, R_w, GOF	0.068, 0.102, 1.269	0.057, 0.079, 1.186	0.090, 0.141, 1.332	0.056, 0.095, 1.446	0.059, 0.111, 1.251	0.082, 0.194, 2.016	0.089, 0.112, 1.087	0.040, 0.061, 0.998	0.034, 0.049, 1.115
max shift in final cycle	0.0030	0.0020	0.1970	0.1270	0.0110	0.0040	0.0110	0.0050	0.0010
final diff map, max, e/Å^3	1.81	1.00	0.78	1.66	1.59	4.42	3.69	1.65	0.62

were collected with the $2\theta/\omega$ scan mode. All data were corrected for absorption (ψ-scan)[22] and extinction.[23] Crystal data for **9** was collected on a Mac Science DIP2030 imaging plate equipped with graphite-monochromated Mo Kα radiation (λ = 0.71073 Å). Unit cell parameters were determined by autoindexing several images in each data set separately with the program DENZO.[24] From the cell constants and systematic absences, the space group was chosen to be $P2_1/a$. For each data set, rotation images were collected in 3° increments with a total rotation of 180° about ϕ. Data were processed by using SCALEPACK.[24] The structures were solved by a direct method with the program Crystan-GM (Mac Science) and by refined full-matrix least squares. All non-hydrogen atoms were refined with anisotropic themal parameters. All hydrogen atoms could be found on a difference Fourier map; these coordinates were included in the refinement with isotropic thermal parameters.

(22) Furusaki, A. *Acta Crystallogr*. **1979**, *A35*, 220.
(23) Katayama, C. *Acta Crystallogr*. **1986**, *A42*, 19.
(24) The program is available from MacScience Co.

Acknowledgment. We thank to Central Glass Co. for supplying us with 1,1-bis(trifluoromethyl)benzyl alcohol. Part of this work was supported by Grants-in Aid for Scientific Research (Nos. 09239103, 09440218, 11166248, 11304044) from the Ministry of Education, Science, Sports, and Culture, Japan.

Supporting Information Available: Positional and thermal parameters and interatomic distances and angles for **4a**, **4b**, **5a**, **5b**, **5d**, **6a**, **7a**, **9**, and **12a**. This material is available free of charge via the Internet at http://pubs.acs.org.

OM000790L